

Engineering Fragile Topology in Photonic Crystals: Topological Quantum Chemistry of Light

María Blanco de Paz,¹ Maia G. Vergniory,^{1,2} Dario Bercioux,^{1,2} Aitzol García-Etxarri,^{1,2,*} and Barry Bradlyn^{3,†}

¹*Donostia International Physics Center, 20018 Donostia-San Sebastian, Spain*

²*IKERBASQUE, Basque Foundation for Science, Maria Diaz de Haro 3, 48013 Bilbao, Spain*

³*Department of Physics and Institute for Condensed Matter Theory,
University of Illinois at Urbana-Champaign, Urbana, IL, 61801-3080, USA*

(Dated: November 9, 2022)

In this Letter, we apply the recently developed theory of “Topological quantum chemistry” to the study of band structures in photonic crystals. We focus on a family of crystals formed by elliptical rods in a triangular lattice. We show that the symmetry of Bloch states in the Brillouin zone can be used to determine the locations of localized photonic Wannier functions, which can be moved between various positions in the unit cell by engineered band inversions. Finally we show that for certain parameter ranges there exist isolated topological bands which do not admit a well-localized Wannier description, representing the first physical instance of “fragile” topology.

Introduction. In recent years, there have been tremendous parallel advances in the fields of both topological electronic materials and engineered photonic crystals. On the one hand, topologically nontrivial band insulators have been discovered [1–6] which feature protected, gapless surface, edge, and hinge [7–13] states, as well as anomalous bulk response functions [14–16]. The interplay between topology and crystal symmetry in these phases has reinvigorated the study of band theory, and resulted in new connections between topology in momentum space and the real-space orbital structure of electronic solids [17–21]. Following Haldane and Raghu’s seminal ideas [22, 23], many of these concepts have also been simultaneously explored in the propagation of photons in periodic dielectric structures (photonic crystals). For instance, photonic analogs of the quantum Hall effect [24, 25], quantum spin-Hall effect [26–28], quantum valley-Hall effect [29], Floquet topological insulators [30–33], mirror-Chern, and quadrupole insulating [34–42] systems have been recently discovered.

Because photons in linear dielectrics are truly noninteracting, and since they can be cheaply and easily engineered with almost any desirable lattice structure, two dimensional photonic crystals are an ideal playground for studying topological band theory. Pioneering work in this field has primarily focused on recreating strong \mathbb{Z}_2 topological insulators in bosonic systems protected by crystal symmetries as a proxy for fermionic time-reversal symmetry [43, 44]. Most prior work has focused on producing chiral or helical edge modes in photonic systems. However, there exist also “fragile” topological phases, which do not have protected edge states [45–49]. This fragile topology is a property of a fixed number of bands, and can be diagnosed by a bulk winding number. A nonzero winding number reflects the inability to define exponentially localized and symmetric orbitals–Wannier functions–in real space using only the basis of states in the topological bands. With the possible exception of twisted bilayer graphene [50, 51], a material realization

of fragile topology has remained elusive.

In this work, we design in a photonic crystal the first known example of fragile topology. Inspired by Ref. [43], we consider a family of photonic crystal structures with a distorted honeycomb lattice of dielectric rods. We show that by changing the position and shape of the dielectric, several different photonic band structures can be realized. To analyze these band structures, we adapt the theory of topological quantum chemistry [18] to the study of photonic band structures. In particular, we use the symmetry of the wavefunctions in our photonic crystals to identify the set of Wannier functions–known as a band representation–associated to each group of bands [19, 52–56]. While photonic Wannier functions and band representations have been introduced previously [57–65], we here explore their topological implications for the first time. We show that there exist a class of structures where the photonic bands cannot support exponentially localized, symmetric Wannier functions, and by computing the bulk winding number we verify that these bands have nontrivial fragile topology.

The structure of this work is as follows: In the next section, we will introduce our family of models, and compute the band structures for a variety of lattice structures. Then, we will determine the symmetry properties of the photonic Bloch functions, and from these determine the positions of the photonic Wannier functions (when they exist) for each crystal structure. This will allow us to identify the parameter range over which our model exhibits fragile topology, which we will verify in the following section by computing the non-Abelian Berry phases of the photonic bands, and extracting the fragile winding number. Finally, we will conclude with an outlook towards future research and applications.

Model. As a starting point for our design, we chose a two-dimensional triangular lattice of lattice constant a_0 with a unit cell of six circular silicon rods ($\varepsilon = 11.7$) of diameter d arranged in a hexagonal pattern. This non-primitive (enlarged) unit cell is necessary, because we

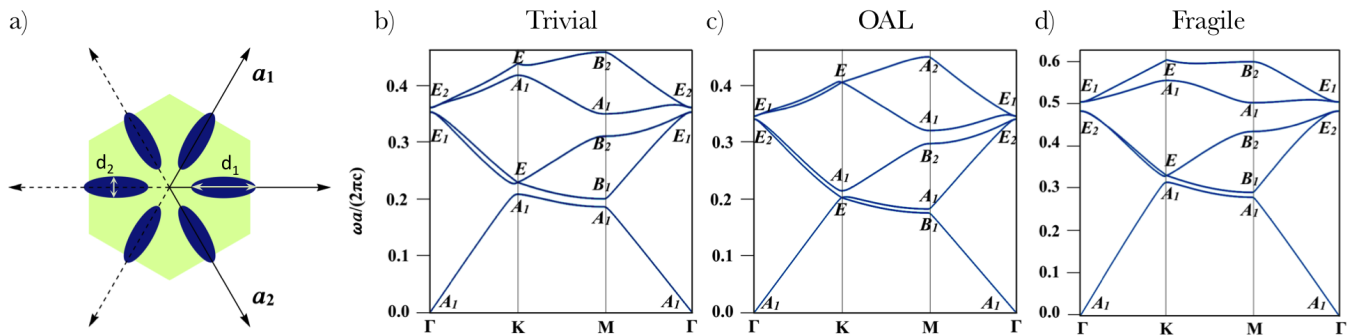


FIG. 1. (a) Schematic showing the real-space unit cell of the structures studied in this work. a_1 and a_2 are the real-space lattice vectors. The centers of the ellipses are fixed at a distance $b = \frac{a_0}{3}$ from the center of the unit cell, a_0 being the lattice constant. d_1 and d_2 are the lengths of the principal axes of the ellipses. Higher dielectric constant shown in blue. When tiling this pattern we use the convention that the dielectric function in any blue region is the same, including when ellipses overlap. b-d) Photonic band structures of three representative examples studied in this work, with little group representations labeled at the high symmetry points. b) Topologically trivial structure, with $d_1 = 0.52a_0$ and $d_2 = 0.31a_0$. c) Band structure of a structure representative of the “obstructed atomic limit” (OAL) phase, with $d_1 = 0.4a_0$ and $d_2 = 0.61a_0$. d) Topologically fragile structure, with $d_1 = 0.4a_0$ and $d_2 = 0.13a_0$.

next distort the rods into ellipses. These ellipses have their principal axes of length d_1 and d_2 , with d_1 oriented in the direction of the lattice vectors (*i.e.* pointing towards the center of the unit cell, see Fig. 1a). The symmetry group of this crystal is the space group $p6mm1'$ (# 183) [66], generated by the lattice translations, sixfold rotational symmetry, mirror reflection about the x -axis, and time-reversal symmetry.

We then computed the band structure for the transverse magnetic (TM) modes in this crystal using the MIT Photonic Bands package (MPB)[67], given by the spectrum of the magnetic wave equation

$$\nabla \times \left(\frac{1}{\epsilon(\mathbf{r})} \times \mathbf{H}(\mathbf{r}) \right) = \left(\frac{\omega}{c} \right)^2 \mathbf{H}(\mathbf{r}), \quad (1)$$

for waves with no propagation in the \mathbf{z} -direction. $\epsilon(\mathbf{r})$ is the position dependent permittivity, $\mathbf{H}(\mathbf{r})$ is the in-plane magnetic field vector, ω is the frequency and c is the speed of light. We show representative band structures for three different cases in Fig. 1. As we will show below, there exists a parameter regime where the second and third bands (counting up from zero energy) are isolated from the rest of the states in the spectrum and exhibit fragile topology.

Photonic Band Representations. As a first step in assessing the topology of bands in our photonic crystal, we will apply the theory of topological quantum chemistry [18] to photonic energy bands. First, we examine the transformation properties of the Bloch eigenstates of our photonic crystal at each of the high symmetry points \mathbf{k}_* (Γ , K , and M) in the Brillouin zone. The group of symmetry operations $G_{\mathbf{k}_*}$ that leaves \mathbf{k}_* invariant is known as the little group of \mathbf{k}_* ; degenerate multiplets of states at each \mathbf{k}_* transform under irreducible representations (irreps) of the group $G_{\mathbf{k}_*}$ [68]. Using the

	Γ	K	M
Trivial	A_1, E_1	A_1, E	A_1, B_1, B_2
OAL	A_1, E_2	E, A_1	B_1, A_1, B_2
Fragile	A_1, E_2	A_1, E	A_1, B_1, B_2

TABLE I. Little group irreps for the three gapped phases of our model. Irreps at each \mathbf{k} -point are ordered from lowest to highest energy. Note that while the OAL and Fragile phases contain the same irreps in the lowest three bands, they differ by a band inversion at K and M .

little group representations given in the Bilbao Crystallographic Server (BCS) [69–71] along with the GTPack package [72, 73], we compute the representation labels at each high symmetry point in our photonic band structure [74]. Using these assignments, we identify three distinct phases of our model by looking at the irreps of the lowest three bands (see Table I, and also the SM).

To extract topological information from the representation labels, recall [18, 56, 59] that for a set of isolated bands $i \in \{1, \dots, N\}$ the symmetry properties of the Bloch-wave eigenstates $\psi_{i\mathbf{k}}(\mathbf{r})$ at every momentum \mathbf{k} in the Brillouin zone are determined by the transformation properties of the Wannier functions

$$w_{i\mathbf{R}}(\mathbf{r}) \equiv \sum_{\mathbf{k}} e^{-i\mathbf{k}\cdot\mathbf{R}} U_{ij}(\mathbf{k}) \psi_{j\mathbf{k}}(\mathbf{r}). \quad (2)$$

Here \mathbf{R} is a lattice vector, and $U_{ij}(\mathbf{k})$ is an $N \times N$ unitary matrix function of \mathbf{k} , and represents a choice of “gauge” for the space spanned by the N -bands. For a topologically trivial set of bands, the matrix U can be chosen to make the functions $w_{n\mathbf{R}}$ exponentially localized about some center $\mathbf{r}_n + \mathbf{R}$. In this case, the Wannier functions transform in a representation of the space group obtained by acting with all elements on the space group on a set of functions at one of the \mathbf{r}_n . These Wannier functions

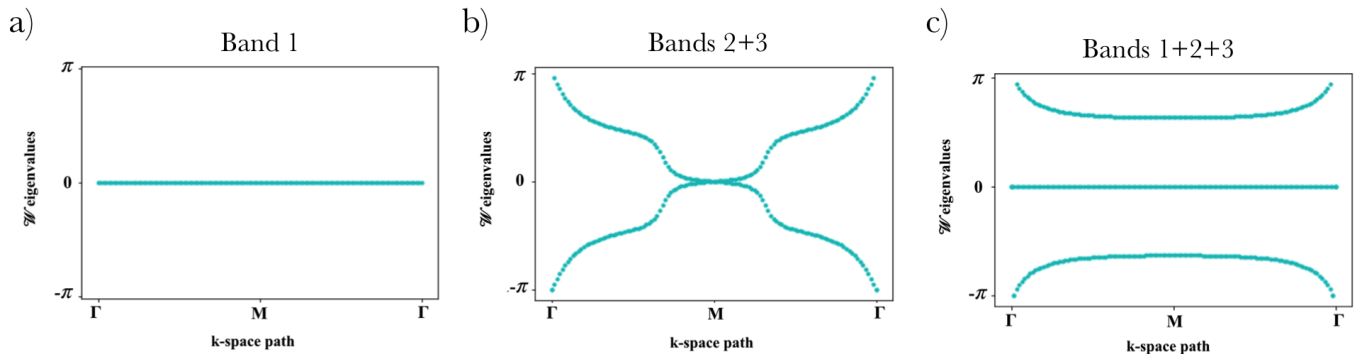


FIG. 2. Wilson loops corresponding to the lowest three in the fragile topological phase. (a) shows the Wilson loop for the isolated first band. The Wilson loop phase here is pinned to $\theta = 0$, a consequence of the C_2 eigenvalues of the band. (b) shows the Wilson loop eigenvalues for the interconnected second and third bands. The Wilson loop spectrum consists of two bands, which wind in opposite directions from $-\pi$ to π . As in Ref. [45], this winding is guaranteed by the C_2 eigenvalues of the bands, and indicates their nontrivial topology. (c) shows the Wilson loop for all three bands taken together, which does not display any winding.

carry a band representation. All band representations can be obtained as a sum of elementary band representations (EBRs), which are tabulated in Ref. [75, 76]. Each EBR is identified by its space group, the Wyckoff position which labels the set \mathbf{r}_n of centers, and an irrep of the group $G_{\mathbf{r}_n}$ which leaves each center invariant (see SM). Inverting this observation, any set of bands that cannot be expressed as a sum of EBRs does not admit exponentially localized and symmetric Wannier functions, and is therefore topological. Note that these considerations apply equally well to both photonic and electronic crystals.

Using the irrep labels given in Table I, along with the catalogue of EBRs in the BCS [69–71], we can identify the band representations describing each phase of our photonic crystal (See Table II of the SM). With $d_1 = 0.52a_0, d_2 = 0.31a_0$, we see that the lowest band carries irrep labels consistent with the band representation $(A_1 \uparrow G)_{1a}$, consisting of photonic Wannier functions centered at the origin with zero angular momentum (s-like). Bands two and three are connected to each other, and are consistent with the $(E_1 \uparrow G)_{1a}$ band representation, with a pair of Wannier functions centered at the origin and transforming like a dipole (p-like). We deem this the “trivial” phase, as all photonic states can be expressed in terms of modes localized near the origin. Note that there are no dielectric rods at the origin, so these Wannier functions are trapped in a symmetric arrangement of dielectrics surrounding the origin. This structure is shown in Fig. 1b. Next, with $d_1 = 0.4a_0, d_2 = 0.61a_0$ we see that the first three bands are all interconnected; taken together, their irrep labels are consistent with s-like photonic Wannier functions centered on a kagome lattice ($3c$ position), and transforming in the $(A_1 \uparrow G)_{3c}$ band representation. Note that this phase was identified in Ref. [43] as possessing a nontrivial topological invariant; here we show that this invariant indicates that the

photonic Wannier functions are localized on a kagome rather than a triangular lattice. In contrast to the trivial phase, the centers of these Wannier functions lie within the dielectric rods. In analogy with similar transitions in electronic materials, we refer to this as the “obstructed atomic limit” (OAL) phase. This band structure is shown in Fig. 1c. Finally, when $d_1 = 0.4a_0, d_2 = 0.1333a_0$ we see that while the lowest band can be described by s-like Wannier functions at the origin of the unit cell, bands two and three cannot be expressed as the sum of EBRs. All three bands taken together, however, contain the same representations as the $(A_1 \uparrow G)_{3c}$ band representation in the OAL phase. This band structure is shown in Fig. 1d. In the following section, we will show that bands two and three in this crystal realize fragile topology [45, 46].

To support these conclusions, for each isolated set of bands we compute the eigenvalues of the Wilson loop

$$W = \mathcal{P}e^{i \oint \mathbf{A} \cdot \mathbf{k}}, \quad (3)$$

where \mathbf{A} is the Berry connection, \mathcal{P} denotes path ordering, and the path of integration goes along a primitive reciprocal lattice vector. As shown in the SM [74], EBRs from each of the different Wyckoff positions in this space group have qualitatively different Wilson loop spectra. Furthermore, the bands in the Wilson loop spectrum for topologically trivial bands do not cover the entire range $[0, 2\pi]$ of possible angles, i.e. they do not wind. We see in Fig. 2a the Wilson loop phase for the lowest band in the fragile topological phase. The phase is pinned at $\phi = 0$, consistent with a Wannier function centered at the $1a$ position. In contrast, the Wilson loop spectrum for the second and third bands, shown in Fig. 2b, clearly possesses nontrivial winding. This is a clear indicator of nontrivial topology.

Fragile Topology. In contrast to a conventional topological insulator, however, the Wilson loop winding in the

fragile phase here is *not* a consequence of time-reversal symmetry. In fact, the crossings in the Wilson loop spectrum at $\mathbf{k}_1 = 0$ and $\mathbf{k}_1 = \pi$ are guaranteed by the twofold rotational symmetry C_{2z} , only due to the limited number of bands considered. Recall that the C_{2z} invariant points in the Brillouin zone are Γ and $M \equiv M' \equiv M''$. Consulting Table I, we see that the C_{2z} eigenvalues of bands two and three at Γ are $(+1, +1)$, while at all three M points they are $(-1, -1)$. As was shown in Refs. [45, 77], this means that the Wilson loop at $\mathbf{k}_1 = 0$, which passes through Γ and M , has its phases pinned to π . Similarly, the Wilson loop at $\mathbf{k}_1 = \pi$ passes through M' and M'' , and so has its phases pinned to 0. This forces the winding of the spectrum in Fig. 2b, and hence the nontrivial topology [74].

In fact, bands two and three realize the same fragile topological phase first discussed in a toy model in Ref. [45]. As in that case, although the irreps at the high symmetry point in our photonic crystal do not match a sum of EBRs, they do match a difference of EBRs. In particular, we can see from the above that the irreps for bands two and three are consistent with the formal difference

$$(A_1 \uparrow G)_{3c} \ominus (A_1 \uparrow G)_{1a},$$

reflecting the fact that all three bands taken together have the same irreps as in the OAL. This reflects the defining feature of fragile topology — that fragile topological bands become trivial when added to topologically trivial bands. We verify this for our model by computing the Wilson loop for all three bands, shown in Fig. 2c. We see that the three-band Wilson loop exhibits no winding, and is consistent with Wannier functions centered at the kagome (3c) position.

Outlook. In this work, we have used the tools of topological quantum chemistry to design and characterize exotic topological photonic crystals. In particular, we have shown that the recently introduced notion of fragile topology arises naturally in photonic crystals with triangular lattice symmetry. Taking inspiration from Refs. [43, 44], we have designed a family of photonic crystals with elliptical rods, which realize trivial, topological, and “obstructed atomic limit” bands as a function of the rod shape. By re-framing photonic band topology in terms of localized Wannier functions, we have shown how concrete topological invariants can be computed without needing to resort to potentially incomplete $\mathbf{k} \cdot \mathbf{p}$ expansions. In Fig. 3, we show the full phase diagram of our model as deduced from irrep ordering. To our knowledge, this represents the first controllable implementation of fragile topology.

We have also highlighted the usefulness of photonic Wannier functions. Because electronic materials are built from the valence electrons localized on atoms, the description of bands in terms of Wannier functions connects directly to the “atomic limit.” The absence of localized

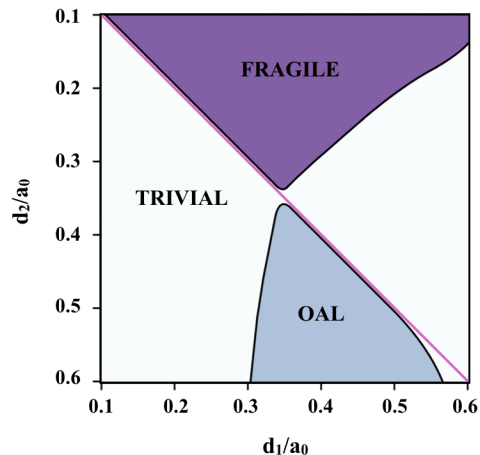


FIG. 3. Phase diagram for the photonic band topology. We show the topological properties of the second and third bands as a function of dielectric displacement and eccentricity. Light blue indicates that the bands form the trivial band representation, Dark blue indicates the obstructed atomic limit (OAL), and Purple indicates the fragile phase. Finally, magenta indicates an intervening gapless phase with fine-tuned degeneracy.

Wannier functions can be thought of as an obstruction to deforming a set of states to a decoupled collection of atomic- or molecular-like orbitals. In photonic crystals, on the other hand, a notion of atomic limit is less clear. Nevertheless, photonic Wannier functions allow for a description of a set of bands in terms of localized resonator modes. These modes may be localized within a single dielectric, or localized by small clusters of dielectric rods (as with modes localized at the origin in our crystal structure). The topological obstruction to forming photonic Wannier functions then manifests itself in localized modes which decay slowly outside of their confining dielectric. A promising avenue for future exploration is the study of how the long tails of the topological Wannier functions influence defect states, and evanescent coupling between external probes and topologically fragile bands in photonic crystals.

Acknowledgments The authors thank G. Giedke and J. J. Saenz, for initial discussions. BB additionally acknowledges discussions with B. Gadway and I. Souza. MG and AGE acknowledge the IS2016-75862-P and FIS2016-80174-P national projects of the Spanish MINECO respectively. AGE received funding from the Fellows Gipuzkoa fellowship of the Gipuzkoako Foru Aldundia through FEDER “Una Manera de hacer Europa”, and $\mu 4F$ (KK-2017/00089) project under the Basque Government ELKARTEK program. The work of MBP, DB and AGE is supported by the Basque Government through the SOPhoQua project (Grant PI2016-41). The work of DB is supported by Spanish Ministerio de Ciencia, Innovación y Universidades (MICINN) under the

project FIS2017-82804-P.

* aitzolgarcia@dipc.org

† bbradlyn@illinois.edu

- [1] D. J. Thouless, M. Kohmoto, M. P. Nightingale, and M. den Nijs, *Physical Review Letters* **49**, 405 (1982).
- [2] C. L. Kane and E. J. Mele, *Phys. Rev. Lett.* **95**, 226801 (2005).
- [3] L. Fu, C. L. Kane, and E. J. Mele, *Phys. Rev. Lett.* **98**, 106803 (2007).
- [4] B. A. Bernevig, T. L. Hughes, and S.-C. Zhang, *Science* **314**, 1757 (2006).
- [5] M. König, S. Wiedmann, C. Brüne, A. Roth, H. Buhmann, L. W. Molenkamp, X.-L. Qi, and S.-C. Zhang, *Science* **318**, 766 (2007).
- [6] Y. Xia *et al.*, *Nature Phys.* **5**, 398 (2009).
- [7] F. Schindler, A. M. Cook, M. G. Vergniory, Z. Wang, S. S. P. Parkin, B. A. Bernevig, and T. Neupert, *Science Advances* **4** (2018), [10.1126/sciadv.aat0346](https://doi.org/10.1126/sciadv.aat0346), <http://advances.sciencemag.org/content/4/6/eaat0346.full.pdf>.
- [8] E. Khalaf, H. C. Po, A. Vishwanath, and H. Watanabe, *Phys. Rev. X* **8**, 031070 (2018).
- [9] W. A. Benalcazar, B. A. Bernevig, and T. L. Hughes, *Science* **357**, 61 (2017).
- [10] W. A. Benalcazar, B. A. Bernevig, and T. L. Hughes, *Physical Review B* **96**, 245115 (2017).
- [11] W. A. Benalcazar, T. Li, and T. L. Hughes, arXiv preprint arXiv:1809.02142 (2018).
- [12] Z. Song, Z. Fang, and C. Fang, *Phys. Rev. Lett.* **119**, 246402 (2017).
- [13] B. J. Wieder, Z. Wang, J. Cano, X. Dai, L. M. Schoop, B. Bradlyn, and B. A. Bernevig, (2018), to appear.
- [14] X.-L. Qi, T. L. Hughes, and S.-C. Zhang, *Physical Review B* **78**, 195424 (2008).
- [15] A. M. Essin, J. E. Moore, and D. Vanderbilt, *Physical review letters* **102**, 146805 (2009).
- [16] J. C. Teo and C. L. Kane, *Physical Review B* **82**, 115120 (2010).
- [17] A. A. Soluyanov and D. Vanderbilt, *Phys. Rev. B* **83**, 035108 (2011).
- [18] B. Bradlyn, L. Elcoro, J. Cano, M. G. Vergniory, Z. Wang, C. Felser, M. I. Aroyo, and B. A. Bernevig, *Nature* **547**, 298 (2017).
- [19] J. Cano, B. Bradlyn, Z. Wang, L. Elcoro, M. G. Vergniory, C. Felser, M. I. Aroyo, and B. A. Bernevig, *Phys. Rev. B* **97**, 035139 (2018).
- [20] J. Höller and A. Alexandradinata, *Phys. Rev. B* **98**, 024310 (2018).
- [21] H. C. Po, A. Vishwanath, and H. Watanabe, *Nat. Comm.* **8**, 50 (2017).
- [22] F. Haldane and S. Raghu, *Physical review letters* **100**, 013904 (2008).
- [23] S. Raghu and F. D. M. Haldane, *Physical Review A* **78**, 033834 (2008).
- [24] Z. Wang, Y. Chong, J. D. Joannopoulos, and M. Soljačić, *Physical review letters* **100**, 013905 (2008).
- [25] Z. Wang, Y. Chong, J. D. Joannopoulos, and M. Soljačić, *Nature* **461**, 772 (2009).
- [26] A. B. Khanikaev, S. H. Mousavi, W.-K. Tse, M. Kargarian, A. H. MacDonald, and G. Shvets, *Nature materials* **12**, 233 (2013).
- [27] M. Hafezi, E. A. Demler, M. D. Lukin, and J. M. Taylor, *Nature Physics* **7**, 907 (2011).
- [28] R. Umucalılar and I. Carusotto, *Physical Review A* **84**, 043804 (2011).
- [29] T. Ma and G. Shvets, *New Journal of Physics* **18**, 025012 (2016).
- [30] K. Fang, Z. Yu, and S. Fan, *Nature photonics* **6**, 782 (2012).
- [31] L. J. Maczewsky, J. M. Zeuner, S. Nolte, and A. Szameit, *Nature communications* **8**, 13756 (2017).
- [32] S. Mukherjee, A. Spracklen, M. Valiente, E. Andersson, P. Öhberg, N. Goldman, and R. R. Thomson, *Nature communications* **8**, 13918 (2017).
- [33] M. C. Rechtsman, J. M. Zeuner, Y. Plotnik, Y. Lumer, D. Podolsky, F. Dreisow, S. Nolte, M. Segev, and A. Szameit, *Nature* **496**, 196 (2013).
- [34] L. Zhang, Y. Yang, P. Qin, Q. Chen, F. Gao, E. Li, J.-H. Jiang, B. Zhang, and H. Chen, arXiv e-prints, arXiv:1901.07154 (2019), [arXiv:1901.07154](https://arxiv.org/abs/1901.07154) [physics.app-ph].
- [35] A. E. Hassan, F. K. Kunst, A. Moritz, G. Andler, E. J. Bergholtz, and M. Bourennane, arXiv preprint arXiv:1812.08185 (2018).
- [36] Y. Ota, F. Liu, R. Katsumi, K. Watanabe, K. Wakabayashi, Y. Arakawa, and S. Iwamoto, arXiv preprint arXiv:1812.10171 (2018).
- [37] B. Y. Xie, H. F. Wang, X. Y. Zhu, M. H. Lu, and Y. F. Chen, arXiv preprint arXiv:1805.07555 (2018).
- [38] L. Lu, C. Fang, L. Fu, S. G. Johnson, J. D. Joannopoulos, and M. Soljačić, *Nature Physics* **12**, 337 (2016).
- [39] L. J. Maczewsky, B. Höckendorf, M. Kremer, T. Biesen-thal, M. Heinrich, A. Alvermann, H. Fehske, and A. Szameit, arXiv preprint arXiv:1812.07930 (2018).
- [40] T. Ozawa, H. M. Price, A. Amo, N. Goldman, M. Hafezi, L. Lu, M. Rechtsman, D. Schuster, J. Simon, O. Zilberberg, *et al.*, arXiv preprint arXiv:1802.04173 (2018).
- [41] A. Slobozhanyuk, S. H. Mousavi, X. Ni, D. Smirnova, Y. S. Kivshar, and A. B. Khanikaev, *Nature Photonics* **11**, 130 (2017).
- [42] L. Lu, J. D. Joannopoulos, and M. Soljačić, *Nature Photonics* **8**, 821 (2014).
- [43] L.-H. Wu and X. Hu, *Phys. Rev. Lett.* **114**, 223901 (2015).
- [44] G. Siroki, P. A. Huidobro, and V. Giannini, *Phys. Rev. B* **96**, 041408 (2017).
- [45] J. Cano, B. Bradlyn, Z. Wang, L. Elcoro, M. G. Vergniory, C. Felser, M. I. Aroyo, and B. A. Bernevig, *Phys. Rev. Lett.* **120**, 266401 (2018).
- [46] H. C. Po, H. Watanabe, and A. Vishwanath, *Phys. Rev. Lett.* **121**, 126402 (2018).
- [47] B. J. Wieder and B. A. Bernevig, arXiv preprint arXiv:1810.02373 (2018).
- [48] J. Ahn and B.-J. Yang, arXiv preprint arXiv:1810.05363 (2018).
- [49] A. Bouhon, A. M. Black-Schaffer, and R.-J. Slager, (2018), [arXiv:1804.09719](https://arxiv.org/abs/1804.09719).
- [50] L. Zou, H. C. Po, A. Vishwanath, and T. Senthil, *Physical Review B* **98**, 085435 (2018).
- [51] Z. Song, Z. Wang, W. Shi, G. Li, C. Fang, and B. A. Bernevig, arXiv preprint arXiv:1807.10676 (2018).
- [52] J. Zak, *Phys. Rev. Lett.* **45**, 1025 (1980).
- [53] J. Zak, *Physical Review B* **23**, 2824 (1981).

- [54] J. Zak, Phys. Rev. B **26**, 3010 (1982).
- [55] H. Bacry, L. Michel, and J. Zak, “Symmetry and classification of energy bands in crystals,” in *Group theoretical methods in Physics: Proceedings of the XVI International Colloquium Held at Varna, Bulgaria, June 15–20 1987* (Springer Berlin Heidelberg, 1988) p. 289.
- [56] L. Michel and J. Zak, Phys. Rep. **341**, 377 (2001).
- [57] K. M. Leung, JOSA B **10**, 303 (1993).
- [58] K. Busch, S. F. Mingaleev, A. Garcia-Martin, M. Schillinger, and D. Hermann, Journal of Physics: Condensed Matter **15**, R1233 (2003).
- [59] K. Busch, C. Blum, A. M. Graham, D. Hermann, M. Köhl, P. Mack, and C. Wolff, Journal of Modern Optics **58**, 365 (2011).
- [60] C. Wolff and K. Busch, Physica B: Condensed Matter **407**, 4051 (2012).
- [61] C. Wolff, P. Mack, and K. Busch, Physical Review B **88**, 075201 (2013).
- [62] D. Whittaker and M. Croucher, Physical Review B **67**, 085204 (2003).
- [63] J. Albert, C. Jouanin, D. Cassagne, and D. Bertho, Physical Review B **61**, 4381 (2000).
- [64] J. Albert, C. Jouanin, D. Cassagne, and D. Monge, Optical and quantum electronics **34**, 251 (2002).
- [65] M. L. V. Dyerville, D. Monge, D. Cassagne, and J. Albert, Optical and quantum electronics **34**, 445 (2002).
- [66] M. I. Aroyo, ed., *International Tables for Crystallography*, Vol. A (International Union of Crystallography, 2016).
- [67] S. G. Johnson and J. D. Joannopoulos, Optics express **8**, 173 (2001).
- [68] C. J. Bradley and A. P. Cracknell, *The Mathematical Theory of Symmetry in Solids* (Clarendon Press, Oxford, 1972).
- [69] M. I. Aroyo, J. M. Perez-Mato, D. Orobengoa, E. Tasci, G. de la Flor, and A. Kirov, Bulg. Chem. Commun. **43(2)**, 183 (2011).
- [70] M. I. Aroyo, J. M. Perez-Mato, C. Capillas, E. Kroumova, S. Ivantchev, G. Madariaga, A. Kirov, and H. Wondratschek, Z. Krist. **221**, 15 (2006).
- [71] M. I. Aroyo, A. Kirov, C. Capillas, J. M. Perez-Mato, and H. Wondratschek, Acta Cryst. **A62**, 115 (2006).
- [72] R. M. Geilhufe and W. Hergert, *Frontiers in Physics* **6**, 86 (2018).
- [73] W. Hergert and R. M. Geilhufe, *Group Theory in Solid State Physics and Photonics: Problem Solving with Mathematica* (Wiley-VCH, 2018) ISBN: 978-3-527-41133-7.
- [74] See Supplementary Material.
- [75] Bilbao Crystallogr. Server, “Bandrep: Band representations of the double space groups,” (2017), <http://www.cryst.ehu.es/cgi-bin/cryst/programs/bandrep.pl>.
- [76] L. Elcoro, B. Bradlyn, Z. Wang, M. G. Vergniory, J. Cano, C. Felser, B. A. Bernevig, D. Orobengoa, G. de la Flor, and M. I. Aroyo, J. Appl. Cryst. **50**, 1457 (2017).
- [77] A. Alexandradinata, C. Fang, M. J. Gilbert, and B. A. Bernevig, *Phys. Rev. Lett.* **113**, 116403 (2014).

Supplementary Material for Engineering Fragile Topology in Photonic Crystals: Topological Quantum Chemistry of Light

María Blanco de Paz,¹ Maia G. Vergniory,^{1,2} Dario Bercioux,^{1,2} Aitzol García-Etxarri,^{1,2} and Barry Bradlyn³

¹*Donostia International Physics Center, 20018 Donostia-San Sebastian, Spain*

²*IKERBASQUE, Basque Foundation for Science, Maria Diaz de Haro 3, 48013 Bilbao, Spain*

³*Department of Physics and Institute for Condensed Matter Theory,
University of Illinois at Urbana-Champaign, Urbana, IL, 61801-3080, USA*

(Dated: November 9, 2022)

CRYSTALLOGRAPHY AND BAND REPRESENTATIONS

All the photonic crystal structures considered in this work have the symmetries of the symmorphic space group $p6mm1'$. The Bravais lattice for this space group is generated by the primitive translations

$$\mathbf{a}_1 = a_0 \frac{1}{2} \hat{\mathbf{x}} + \frac{\sqrt{3}}{2} \hat{\mathbf{y}}, \quad \mathbf{a}_2 = a_0 \frac{1}{2} \hat{\mathbf{x}} - \frac{\sqrt{3}}{2} \hat{\mathbf{y}}. \quad (1)$$

The point group is isomorphic to $C_{6v}(6mm)$ and is generated by a sixfold rotation C_6 about the origin, as well as the mirror reflection m_y which interchanges \mathbf{a}_1 and \mathbf{a}_2 . In Fig. 1a we show the unit cell for this space group. Points within the unit cell fall into orbits under the action of the space group, known as Wyckoff positions. We have labelled several of the Wyckoff positions relevant to this work. First, the $1a$ position has reduced coordinates $\mathbf{q}_{1a} = (0, 0)$. The site symmetry group G_{1a} which leaves the $1a$ position invariant is isomorphic to the full point group C_{6v} . Applying the lattice translations to the $1a$ position yields a triangular lattice. Next, the $2b$ position has multiplicity 2, with reduced coordinates $\{\mathbf{q}_{2b}^1, \mathbf{q}_{2b}^2\} = \{(1/3, 2/3), (2/3, 1/3)\}$. The operation m_y interchanges \mathbf{q}_{2b}^1 and \mathbf{q}_{2b}^2 ; the site symmetry group G_{2b} of each point in the $2b$ position is thus isomorphic to the point group C_{3v} consisting of a threefold rotation and a mirror symmetry C_6m_y . Applying the lattice translations to the points in the $2b$ Wyckoff position yields a honeycomb lattice. Next, the $3c$ position has multiplicity 3, with reduced coordinates $\{\mathbf{q}_{3c}^1, \mathbf{q}_{3c}^2, \mathbf{q}_{3c}^3\} = \{(1/2, 0), (0, 1/2), (1/2, 1/2)\}$. C_3 symmetry acts to permute these points, and the stabilizer group G_{3c} of each is isomorphic to the point group C_{2v} . These exhaust the maximal Wyckoff positions for this space group. Lastly, we indicate in the figure the non-maximal $6d$ Wyckoff position. This position has multiplicity 6, and lies along the lines connecting the $1a$ and $3c$ Wyckoff positions. The elliptical rods we consider here are placed at the $6d$ position.

Next, we consider the Brillouin zone. We take as a basis for the reciprocal lattice the vectors

$$\mathbf{g}_1 = \frac{4\pi}{a_0\sqrt{3}} \left(\frac{\sqrt{3}}{2} \hat{\mathbf{x}} + \frac{1}{2} \hat{\mathbf{y}} \right), \quad \mathbf{g}_2 = \frac{4\pi}{a_0\sqrt{3}} \left(\frac{\sqrt{3}}{2} \hat{\mathbf{x}} - \frac{1}{2} \hat{\mathbf{y}} \right) \quad (2)$$

Within the Brillouin zone, there are three main classes of high symmetry points with nontrivial little group. First, the Γ point has reduced coordinates $(0, 0)$, and has as its little group the full space group. Next, there are the two K points K and K' with reduced coordinates $(1/3, 1/3)$ and $(2/3, 2/3)$ respectively. The little group of these points is isomorphic to the space group $p3m1$, with point group C_{3v} . Note also that the K points are not invariant under time-reversal symmetry. Finally, we have the three M points $M, M',$ and M'' with reduced coordinates $(1/2, 0), (0, 1/2),$ and $(1/2, 1/2)$ respectively. The little group of these points is isomorphic to the space group $p2mm1'$, with point group C_{2v} . We show the Brillouin zone with high-symmetry points labelled in Fig. 1b.

Recall that Bloch functions at high-symmetry momenta \mathbf{k}_* transform in irreducible representations of the little group $G_{\mathbf{k}_*}$ of \mathbf{k}_* . Furthermore, Wannier functions exponentially localized at a high-symmetry Wyckoff position \mathbf{q} transform in irreducible representations of the stabilizer group $G_{\mathbf{q}}$ of \mathbf{q} . Since the space group $p6mm1'$ is symmorphic, both site symmetry and little group irreps can be labelled by irreps of point groups; in this space group, we have seen above that the relevant point groups are $C_{2v}, C_{3v},$ and C_{6v} . In Table I we give the character tables for these representations, which are referred to frequently in the main text.

Finally, recall that for a set of bands spanned by exponentially localized, symmetric Wannier functions, the irreps of the little group at high symmetry points in the Brillouin zone are fully determined by the irreps of the site-symmetry group under which the Wannier functions transform. Such a set of bands is a *band representation*, as defined in Refs. [1–3]. Any band representation can be expressed as a sum of *elementary band representations* (EBRs), each of

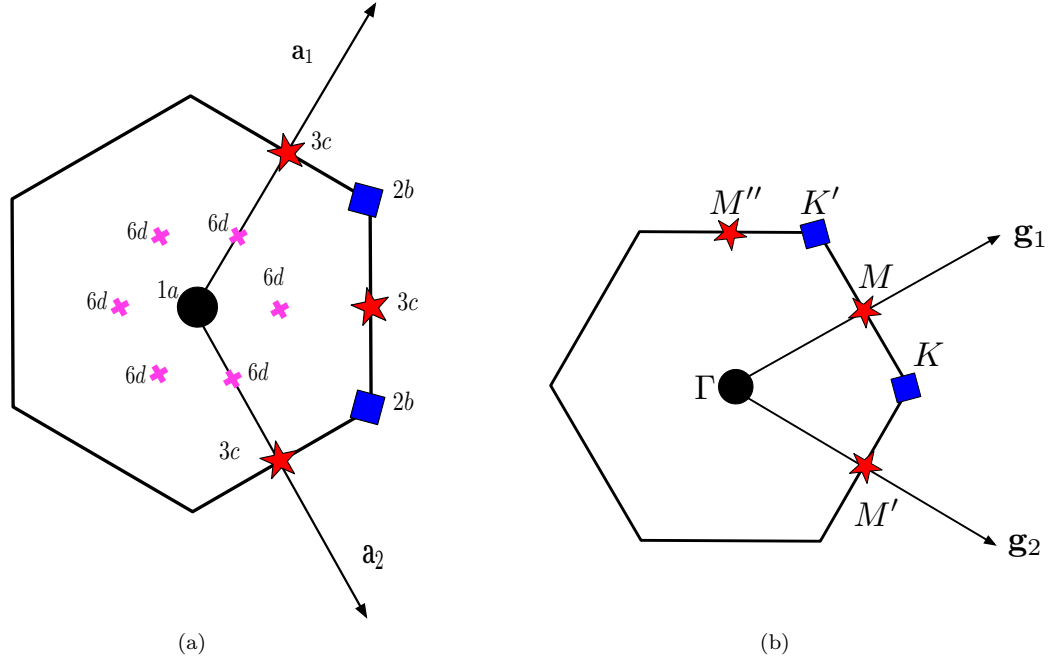


FIG. 1. Unit cell and first Brillouin zone for $p6mm1'$. (a) Shows the real space unit cell with relevant Wyckoff positions labelled. The $1a$ position is indicated by a black circle, the $2b$ position by blue squares, the $3c$ position by red stars, and the $6d$ position by pink crosses. (b) shows the first Brillouin zone with the high symmetry Γ , M , and K points labelled. Note that little group and site symmetry representations of points labelled by black circles are given by irreps of C_{6v} . Irreps for all blue squares are given by labels for C_{3v} . Irreps for all red stars are given by labels for C_{2v} .

ρ	E	C_2	m_1	m_2
A_1	1	1	1	1
A_2	1	1	-1	-1
B_1	1	-1	-1	1
B_2	1	-1	1	-1

(a)

ρ	E	m	C_3
A_1	1	1	1
A_2	1	-1	1
E	2	0	-1

(b)

ρ	E	m_1	C_2	C_3	m_2	C_6
A_1	1	1	1	1	1	1
A_2	1	-1	1	1	-1	1
B_1	1	-1	-1	1	1	-1
B_2	1	1	-1	1	-1	-1
E_1	2	0	-2	-1	0	1
E_2	2	0	2	-1	0	-1

(c)

TABLE I. Character tables for the point groups used in this work. (a) is the character table for C_{2v} , which labels representations of both G_{3c} , the stabilizer group of the $3c$ position, as well as of the little groups $G_M, G_{M'}$, and $G_{M''}$ of the M points. (b) is the character table for C_{3v} , which labels representations of both G_{2b} , the stabilizer group of the $2b$ position, as well as of the little groups G_K and $G_{K'}$ of the K points. (c) is the character table for C_{6v} which labels representations of both G_{1a} , the stabilizer group of the $1a$ position, as well as of the little group G_Γ of the Γ point.

which is defined by a maximal Wyckoff position (in this case, $1a$, $2b$, or $3c$), along with an irrep of the corresponding site-symmetry group. These will be denoted

$$(\rho \uparrow G)_{\mathbf{q}}, \quad (3)$$

where ρ is an irrep of the site symmetry group $G_{\mathbf{q}}$ of the Wyckoff position \mathbf{q} . Since each EBR contains a finite number of bands, we can define a direct sum \oplus of EBRs by concatenating bands; the multiplicities of little group irreps appearing in a sum of EBRs is a sum of the multiplicities in each EBR. Similarly, at the level of little group irreps we can define a formal difference of EBRs[4, 5] as well. We define

$$\mathcal{S} \equiv (\rho_1 \uparrow G)_{\mathbf{q}_1} \ominus (\rho_2 \uparrow G)_{\mathbf{q}_2} \quad (4)$$

to be the set of little group irrep multiplicities that one obtains by subtracting the irrep multiplicities in $(\rho_2 \uparrow G)_{\mathbf{q}_2}$ from those in $(\rho_1 \uparrow G)_{\mathbf{q}_1}$. The full set of elementary band representations for all space groups can be found in Ref. [6]. Below in Table II we give the little group irreps which appear in the EBRs relevant to this work.

EBR	Γ	K	M
$(A_1 \uparrow G)_{1a}$	A_1	A_1	A_1
$(E_1 \uparrow G)_{1a}$	E_1	E	$B_1 \oplus B_2$
$(A_1 \uparrow G)_{3c}$	$A_1 \oplus E_2$	$E \oplus A_1$	$A_1 \oplus B_1 \oplus B_2$

TABLE II. EBRs appearing in the lowest three bands of our photonic crystal structures. The first column gives the label of the EBR. The second column gives the little group irreps describing bands at Γ in the EBR. Similarly, third column gives the little group irreps describing bands at K , and the fourth column the irreps for bands at M .

REVIEW OF WILSON LOOPS

In this section, we recall some facts about Wilson loops which are used in the main text. We will also prove the quantization results used in the main text, in the interest of creating a self-contained work. The Wilson loop matrix

$$W(k_1) = \mathcal{P} \exp \left(i \oint A_2(k_1, k_2) dk_2 \right) \quad (5)$$

can be discretized as a numerically tractable product

$$W(k_1)_{mn} = \langle u_{m,(k_1,\pi)} | \prod_{k_2}^{\pi \leftarrow -\pi} P(k_1, k_2) | u_{n,(k_1,-\pi)} \rangle \quad (6)$$

where we have introduced the projector $P(\mathbf{k}) = \sum_n |u_{n\mathbf{k}}\rangle \langle u_{n\mathbf{k}}|$ onto a set of disconnected bands, and the infinite path ordered product is shorthand for

$$\prod_{k_2}^{\pi \leftarrow -\pi} P(k_1, k_2) = \lim_{\Delta \rightarrow 0} P(k_1, \pi) P(k_1, \pi - \Delta) \cdots P(k_1, \Delta) P(k_1, -\pi) \quad (7)$$

The Wilson loop is a unitary matrix, and the phases $\{\theta_i\} = -i \text{spec}(\log W)$ of its eigenvalues are gauge-invariant modulo 2π . These phases give the centers of hybrid Wannier functions (functions localized in the \mathbf{a}_2 direction and extended in the \mathbf{a}_1 direction) supported by the bands in the image of the projectors P [7, 8].

In the case when we evaluate the Wilson loop for a small number of bands, the irreps of the Bloch functions at high symmetry momenta can place constraints on the allowed phases $\{\theta_i\}$. First note that our photonic crystals have both C_2 rotation and time reversal (T) symmetries. The combined symmetry C_2T is antiunitary, and leaves all \mathbf{k} points invariant. Since each projector $P(\mathbf{k})$ is C_2T invariant, the net effect of this symmetry on the Wilson loop is to take $W(\mathbf{k}_1)$ to itself. Imposing this symmetry, and recalling that it is antiunitary, we deduce that $W(\mathbf{k})$ and $W^*(\mathbf{k})$ must have the same spectrum. The phases θ_i thus come in pairs $\{\theta_i, -\theta_i\}$, or else $\theta_i = 0, \pi$. If we compute this Wilson loop for a single isolated band, it must have either $\theta = 0$ or $\theta = \pi$.

In the case of one or two occupied bands, we can determine $\{\theta_i\}$ solely from the eigenvalues of C_2 symmetry at Γ and M . To see this, let us consider first $W(0)$. Starting with the definition Eq. (7) and splitting the product in half, we find

$$W(0) = \langle u_{m,(0,\pi)} | \prod_{k_2}^{\pi \leftarrow -\pi} P(0, k_2) | u_{n,(0,-\pi)} \rangle \quad (8)$$

$$= \langle u_{m,(0,\pi)} | \prod_{k_2}^{\pi \leftarrow 0} P(0, k_2) | u_{\ell,(0,0)} \rangle \langle u_{\ell,(0,0)} | \prod_{k_2}^{0 \leftarrow -\pi} P(0, k_2) | u_{n,(0,-\pi)} \rangle \quad (9)$$

$$\equiv W_{\pi \leftarrow 0}(0) W_{0 \leftarrow -\pi}(0) \quad (10)$$

Now, with C_2 symmetry we can write

$$C_2 |u_{m,(0,-\pi)}\rangle = |u_{n,(0,\pi)}\rangle \mathcal{B}_M^{nm}(C_2), \quad (11)$$

$$C_2 |u_{m,(0,0)}\rangle = |u_{n,(0,0)}\rangle \mathcal{B}_\Gamma^{nm}(C_2), \quad (12)$$

where $\mathcal{B}_\Gamma^{mn}(C_2)$ and $\mathcal{B}_M^{mn}(C_2)$ is the matrix representations of C_2 at the Γ and M points, respectively. Inserting the identity operator C_2^2 in the expression for $W_{0 \leftarrow -\pi}$ and using the invariance of the projectors, we find

$$W_{0 \leftarrow -\pi}(0) = \mathcal{B}_\Gamma(C_2) W_{\pi \leftarrow 0}^\dagger(0) \mathcal{B}_M(C_2) \quad (13)$$

and so

$$W(0) = W_{\pi \leftarrow 0}(0) \mathcal{B}_\Gamma(C_2) W_{\pi \leftarrow 0}^\dagger(0) \mathcal{B}_M(C_2) \quad (14)$$

We can apply similar considerations to $W(\pi)$ to deduce

$$W(\pi) = W_{\pi \leftarrow 0}(\pi) \mathcal{B}_M(C_2) W_{\pi \leftarrow 0}^\dagger(\pi) \mathcal{B}_{M''}(C_2) \quad (15)$$

These expressions are particularly useful when the representation matrices $\mathcal{B}(C_2)$ are proportional to the identity matrix. This is always true in the case of one or two occupied bands for the irreps in Table II. In this case, we have

$$W(0) = \text{sign}(\chi_\Gamma(C_2)\chi_M(C_2))\mathbb{I} \quad (16)$$

$$W(\pi) = \mathbb{I}, \quad (17)$$

where $\chi(C_2)$ is character of C_2 in each little group irrep, and \mathbb{I} is the appropriately sized identity matrix. From this formula two observations used in the main text follow immediately:

1. For a single isolated band, the little group irreps at Γ and M have the same C_2 eigenvalues. This Wilson loop will be pinned to $\theta = 0$. This encompasses the case of the $(A_1 \uparrow G)_{1a}$ band representation observed in our fragile photonic crystal.
2. For two isolated bands with a single irrep at Γ and M , the Wilson loop at $k_1 = 0$ will be pinned to 0 if the irreps have the same C_2 eigenvalues, and will be pinned to π in the case that the irreps have opposite C_2 eigenvalues. In this latter case, the Wilson loop must wind so that $W(\pi)$ has $\theta_1 = \theta_2 = 0$. This is what occurs for the fragile topological bands.

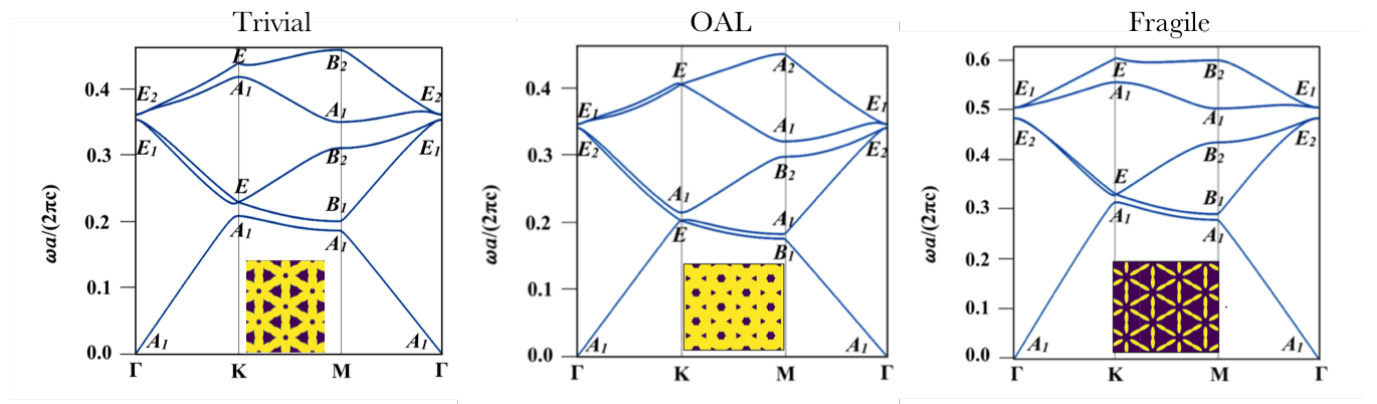


FIG. 2. Band structures for trivial, fragile, and obstructed atomic limit structures. Inset shows the periodic arrangement of dielectric rods.

NUMERICAL METHODS

Here we describe the methods used to calculate the photonic band structures. We first define a scan of 300 by 300 structures varying the values of the axes of the ellipses, d_1 and d_2 , from $0.1a_0$ to $0.7a_0$. All ellipses are then placed at a distance of $a_0/3$ from the center of the triangular unit cell. Next, we use the program MIT Photonic-Bands (MPB)[9] to solve the eigenvalue problem and get the band structure and the eigenvectors at the high symmetry points (Γ , K and M). We then determine the symmetry of the Bloch functions using GTPack[10, 11], taking into account the little group of the high symmetry points. Once we have the irreps for the first three bands, the structures can be classified into trivial, fragile or OAL by symmetry. If the phase is fragile, for Γ the representations must be: A_1, E_2 , and for K : A_1, E . If it is OAL, the irreps on Γ are the same but on K are inverted: E, A_1 (see main text). Any other combination of irreps gives either a trivial or a gapless phase. To further refine this classification, we exclude symmetry-allowed band crossings at high symmetry points. This allows us to build the phase diagram in Fig. 3 in the main text. From

the phase diagram, we picked one representative structure for each phase. Band structures and real space structures for these phases are shown in Fig. 2.

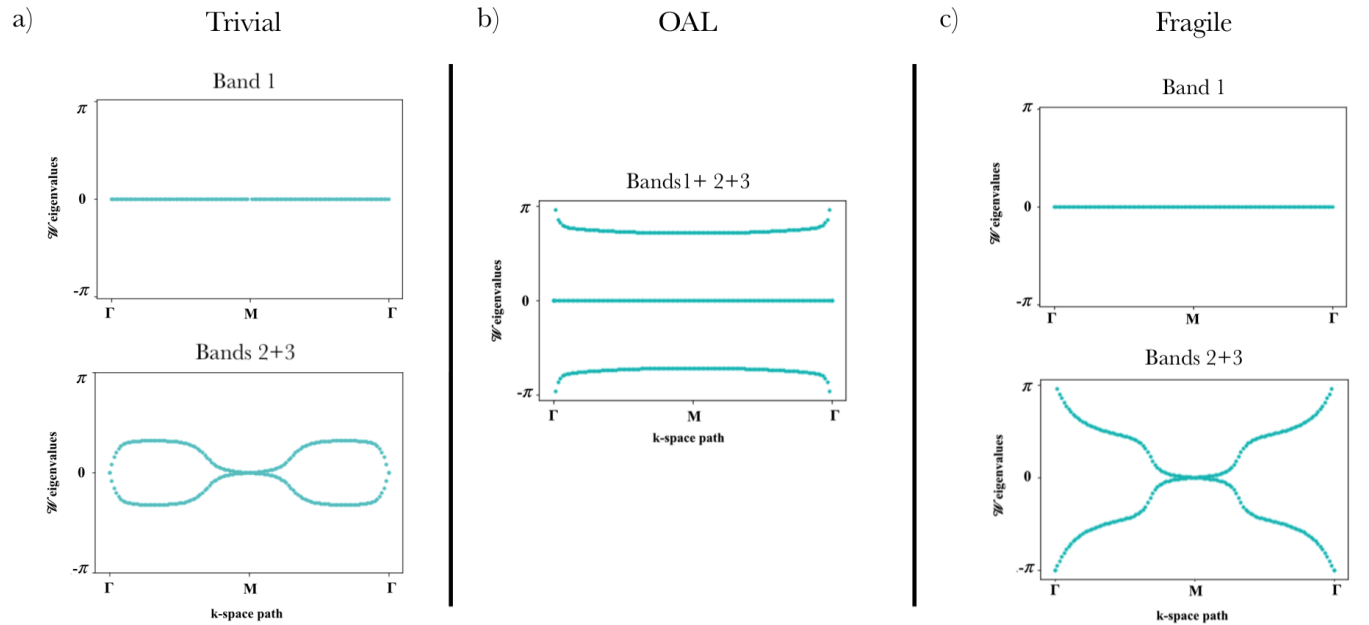


FIG. 3. Wilson loops for the trivial, fragile and OAL structures. (a) shows the Wilson loop for bands 1, bands 2 and 3, and bands 1,2 and 3 for the trivial structure. (b) shows the same loops for the fragile structure. (c) shows the Wilson loop for the three lowest bands in the obstructed atomic limit structure.

To compute the Wilson loops, we use the discretized formula Eq. (6) presented above for a fixed Δ , following the algorithm of Marzari and Vanderbilt[7]. We enforce the boundary conditions

$$u_{n\mathbf{k}+\mathbf{G}}(\mathbf{r}) = e^{-i\mathbf{G}\cdot\mathbf{r}}u_{n\mathbf{k}}(\mathbf{r}), \quad (18)$$

which ensures that the Bloch wavefunctions $\psi_{n\mathbf{k}}(\mathbf{r})$ are periodic functions of \mathbf{k} . We then numerically compute the overlap matrices

$$M_{mn}(\mathbf{k}) = \langle u_{m\mathbf{k}+\Delta\mathbf{g}_2} | u_{n\mathbf{k}} \rangle \quad (19)$$

Multiplying these matrices together along a line $k_2 \in [0, 2\pi]$ gives the Wilson loop matrix $W(k_1)$. We then diagonalize this matrix

$$W(k_1) = UDU^\dagger \quad (20)$$

and compute $\{\theta_i\} = \text{Im} \log D$. In Fig 3 We show the Wilson loop spectra for the Trivial and OAL band structures discussed in the main text.

-
- [1] J. Zak, Phys. Rev. B **26**, 3010 (1982).
 - [2] R. A. Evarestov and V. P. Smirnov, *Site Symmetry in Crystals* (Springer, 1997).
 - [3] B. Bradlyn, L. Elcoro, J. Cano, M. G. Vergniory, Z. Wang, C. Felser, M. I. Aroyo, and B. A. Bernevig, Nature **547**, 298 (2017).
 - [4] Z. Song, Z. Wang, W. Shi, G. Li, C. Fang, and B. A. Bernevig, arXiv preprint arXiv:1807.10676 (2018).
 - [5] B. Bradlyn, Z. Wang, J. Cano, and B. A. Bernevig, Physical Review B **99**, 045140 (2019).
 - [6] Bilbao Crystallogr. Server, “Bandrep: Band representations of the double space groups,” (2017), <http://www.cryst.ehu.es/cgi-bin/cryst/programs/bandrep.pl>.
 - [7] N. Marzari and D. Vanderbilt, Physical review B **56**, 12847 (1997).
 - [8] A. Alexandradinata, C. Fang, M. J. Gilbert, and B. A. Bernevig, Phys. Rev. Lett. **113**, 116403 (2014).

- [9] S. G. Johnson and J. D. Joannopoulos, *Optics express* **8**, 173 (2001).
- [10] R. M. Geilhufe and W. Hergert, *Frontiers in Physics* **6**, 86 (2018).
- [11] W. Hergert and R. M. Geilhufe, *Group Theory in Solid State Physics and Photonics: Problem Solving with Mathematica* (Wiley-VCH, 2018) ISBN: 978-3-527-41133-7.